Translational Oncology
www.transonc.com

Volume 11 Number 3 June 2018 pp. 672–685 672

3D Imaging Detection of HER2 Based in the Use of Novel Affibody-Quantum Dots Probes and Ratiometric Analysis

Perla Pérez-Treviño, Héctor Hernández-De la Cerda, Jorge Pérez-Treviño, Oscar Raúl Fajardo-Ramírez, Noemí García and Julio Altamirano

Tecnologico de Monterrey, Escuela de Medicina, Av. Morones Prieto No. 3000 Pte., Monterrey, NL, Mexico, 64710

Abstract

Patients with breast cancer (BC) overexpressing HER2 (HER2+) are selected for Trastuzumab treatment, which blocks HER2 and improves cancer prognosis. However, HER2+ diagnosis, by the gold standard, immunohistochemistry, could lead to errors, associated to: a) variability in sample manipulation (thin 2D sections), b) use of subjective algorithms, and c) heterogeneity of HER2 expression within the tissue. Therefore, we explored HER2 3D detection by multiplexed imaging of Affibody-Quantum Dots conjugates (Aff-QD), ratiometric analysis (RMA_{FI}) and thresholding, using BC multicellular tumor spheroids (BC-MTS) (~120 μm of diameter) as 3D model of BC. HER2+, HER2– and hybrid HER2+/– BC-MTS (mimicking heterogeneous tissue) were incubated simultaneously with two Aff-QD probes (anti-HER2 and negative control (NC), respectively, (1:1)). Confocal XY sections were recorded along the Z distance, and processed by automatized RMA_{FI} (anti-HER2 Aff-QD/ NC). Quantifying the NC fluorescence allowed to predict the fraction of non-specific accumulation of the anti-HER2 probe within the thick sample, and resolve the specific HER2 level. HER2 was detected up to 30 μm within intact BC-MTS, however, permeabilization improved detection up to 70 μm. Specific HER2 signal was objectively quantified, and HER2 3D-density of 9.2, 48.3 and 30.8% were obtained in HER2−, HER2+ and hybrid HER2+/− permeabilized BC-MTS, respectively. Therefore, by combining the multiplexing capacity of Aff-QD probes and RMA_{FI}, we overcame the challenge of non-specific probe accumulation in 3D samples with minimal processing, yielding a fast, specific spatial HER2 detection and objective quantification.

Translational Oncology (2018) 11, 672–685

Introduction

Human Epidermal Growth Factor Receptor 2 (HER2) is a member of the transmembrane tyrosine kinase receptors, which, under normal conditions, participate in regulating cell growth, survival, differentiation, proliferation, substrate adhesion, motility, etc. [1,2]. Nevertheless, HER2 overexpression (HER2+), which is present in nearly 20% of all breast cancer (BC) cases [3,4], is associated with bad prognosis for the patient due to increased proliferation, invasiveness, regional and distal metastasis and reduction of apoptosis [1,2]. Specific anti-HER2 therapy, based on the use of the monoclonal antibody (AB) Trastuzumab, could improve BC prognosis [5]. However, the use of Trastuzumab is correlated with high incidence of cardiotoxicity [6,7], therefore, its recommendation is highly dependent on accurate diagnosis of the HER2 status [8].

HER2+ BC is diagnosed following a primary screening by immunohistochemistry (IHC) methods, according to the American Society of Clinical Oncology/ College of American Pathologists (ASCO/CAP) guidelines [9], where HER2 in the plasma cell membrane is recognized by a primary monoclonal AB and detected with a secondary AB and a chromogen reaction, using FDA aproval testing kits [10]. Nevertheless, IHC methods could lead to errors on HER2 status diagnosis [8,10–12], with a discordance degree of nearly 20% observed between local and central laboratories [8]. The main causes of IHC errors identified are I) variability in procedures and

Address all correspondence to: Julio Altamirano, Tecnologico de Monterrey, Escuela de Medicina, Av. Morones Prieto No. 3000 Pte., Monterrey, NL, Mexico, 64710.
E-mail:; altamirano@itesm.mx
Received 21 December 2017; Revised 8 March 2018; Accepted 12 March 2018

1936-5233
https://doi.org/10.1016/j.tranon.2018.03.004

extensive sample manipulation to obtain thin 2D sections (3–5 μm) from the formalin-fixed, paraffin-embedded (FFPE) thick tissue samples, deparaffinization, blocking, long staining process and wash off, all of which can alter the sample; II) the operator-dependent semi-quantitative score system used to manually assess the result [8,9,11–13]; and III) BC tumor heterogeneity, where HER2 density could present a variability of ~17% within the same tissue section [13,14].

Efforts in the search of novel reporters and recognition molecules to achieve rapid and more accurate HER2 status for BC diagnosis, with less sample processing, preferentially in thick specimens, or that could be applied directly *in vivo*, without major disturbances, continue to be an important challenge, where false positive signals produced by non-specifically accumulation of the probes could be a typical problem [15,16]. In this context, the use of Quantum Dots (QD), as fluorescent reporters, conjugated with AB, have been used to explore specific HER2 detection [17–20]. QD are fluorescent nanoparticles (10–20 nm), made from inorganic semiconductors, characterized by their unique optical properties, like a large stokes shift, high quantum yield and stability against photobleaching and, more importantly, their multiplexing capacity (since different color QD could be excited simultaneously with the same wavelength, while emitting in different regions of the spectrum), allowing the simultaneous detection of multiple molecular targets using QD with different emission wavelengths [21]. Multiplexing of QD has been widely applied for the simultaneous detection of HER2 and/ or other molecular targets [17,19,20,22], however, most of those studies have focused on the use of primary AB antigen recognition, followed by a secondary detection based in the use of streptavidin or AB conjugated with QD, and analysis of 2D samples is a commonplace.

More recently, QD-based probes have been developed upon conjugation with novel synthetic, molecular recognition proteins, called Affibody molecules (Aff), and have been successfully used for *in vivo* recognition of HER2 in mice with BC xenotransplants [23], or for *in vitro* assessment of HER2 overexpression in monolayer cell cultures [24]. Aff have emerged as a prominent promise for health sciences and biotechnology, because, they are endowed with high affinity and specificity, comparable with traditional monoclonal AB, but with smaller size (6 kDa, compared with the 150 kDa of a typical AB) and simpler structure (three-helix bundle of 58 amino acids, a Z domain) [25,26]. The latter allows its production by recombinant engineering or chemical synthesis, which implies a less expensive recognition molecule available for cancer diagnosis and therapy, when compared with the high cost of monoclonal AB production [25,26]. Although Aff have been extensively explored for *in vivo* HER2 diagnosis [25,27–29], to the best of our knowledge, probes based in Aff and QD have not been used for HER2 assessment in 3D biological samples with minimum processing, aiming to supersede IHC techniques applied in 2D samples, which until now remains as the gold standard for HER2 detection [9].

We took advantage of the multiplexing optical capability of QD, combined with the promising recognition Aff, to objectively detect and quantify HER2 in 3D biological samples. First, using commercially available Aff and QD, we generated two hybrid Aff-QD probes; one specific for HER2 (AffantiHER2-QD605) and other that recognizes the Taq polymerase, and was used as negative control (Affneg-QD545). Both probes were used simultaneously, and the negative control Aff-QD allowed to infer the non-specific accumulation of the probes within the sample. Multicellular tumor spheroids (MTS) of BC cell lines (BC-MTS) were used as 3D model of BC, where the cell–cell and cell-matrix interactions allowed us to approach the complex structure of relatively thick biological samples, as tumors biopsies [30]. The fluorescence signal produced by non-specific accumulation of both Aff-QD probes within BC-MTS was removed by ratiometric analysis (RMA_{FI}), and thresholding, allowed the objective and specific HER2 signal quantification in 3D regions of BC-MTS (HER2 3D-density), where the physical sectioning, in typical IHC, was replaced by optical scanning of 2D sections in the Z distance of the BC-MTS by confocal microscopy.

Material and Methods

Cell Lines and Materials

Estrogen receptor (ER) negative/ HER2 overexpressed (HCC1954) and ER positive/ HER2 basal-expressed (MCF-7) BC cell lines were acquired from the American Type Culture Collection (ATCC) (VA, USA). QDot 605 ITK amino PEG (QD605) (Cat. Q21501MP) and QDot 545 ITK amino PEG (QD545) (Cat. Q21591MP) were obtained from Invitrogen (CA, USA). Anti-ERBB2 Affibody molecule imaging agent (Aff anti HER2 (Affanti-HER2)) (Cat. AB89832), Affibody molecule imaging agent negative control (Aff negative control (Affneg)) (Cat. AB214799), Anti-ERBB2 Affibody molecule (dimeric Aff anti HER2 (AffantiHER2-dim)) (Cat. AB31889) and DRAQ5 fluorophore (Cat. AB108410) were obtained from Abcam (MA, USA). Ultraview universal DAB detection IHQ kit (Cat. 760–500) and the Pathway anti-HER-2/neu (4B5) rabbit monoclonal primary AB (CAT. 790–2991) were acquired from Ventana medical system Inc. (AZ, USA). NAP-5 columns (Cat. 17–0853-01) and NAP-10 columns (Cat. 17–0854-01) were obtained from GE Healthcare (Little Chalfont, UK). Dulbecco's Modified Eagle Medium: Nutrient Mixture F-12 (DMEM/ F-12) (Cat. 12,500–062), Gibco RPMI 1640 medium (Cat. 23,400,021), Phosphate Buffered Saline (PBS) pH 7.2 (10X) (Cat. 70,013–032), Gibco Anti-Anti (100X) solution containing 10,000 U Penicillin/ 10 mg Streptomycin/ 25 μg Fungizone/ ml (Cat. 15,240–062), and laminin mouse protein (Cat. 23,017,015) were purchased from Thermo Fisher Scientific (MA, USA). Fetal Bovine Serum (FBS) (Cat. 35–010-CV) and ultra-low attachment 6 wells plates (Cat. CLS3471) were obtained from Corning (NY, USA). 4-(*N*-Maleimidomethyl) cyclohexanecarboxylic acid *N*-hydroxysuccinimide ester (SMCC) (Cat. M5525), Dimethyl sulfoxide (DMSO) (Cat. D4540), 1,4-Dithiothreitol (DTT) (Cat. 10,197,777,001), ethylene diamine tetra-acetic acid (EDTA) (Cat. EDS), Paraformaldehyde (PFA) (Cat. 158,127), bovine serum albumin (BSA) (Cat. A2058) and *ß*-mercaptoethanol (Cat. M6250) were purchased from Sigma-Aldrich (MO, USA). Cover glasses 25 mm (Cat. C5-25R) were obtained from Warner Instruments (CT, USA) and 0.22 μm membrane filters (Cat. GSWP) from Merck Millipore (MA, USA).

Monolayer Cells and Breast Cancer Multicellular Tumor Spheroids Culture

BC cell lines HCC1954 and MCF-7 were used as HER2+ (positive for HER2 overexpression) [31,32] and HER2– (negative for HER2 overexpression) [33,34], respectively. Both cell types were selected for their capacity to grow in monolayer culture when attached to a substrate, and to grow in suspension culture [35,36]. Cells were cultured in monolayer (1.5×10^5) in sterile cover glasses previously treated with laminin (1.5 μg/ cm^2). HCC1954 cells were grown in RPMI-1640 medium supplemented with 10% FBS and 1% Anti-

Anti [31]. MCF-7 cells were cultured in DMEM/ F-12 supplemented with 10% FBS and 1% Anti-Anti [33]. HER2+ and HER2– BC-MTS were obtained from 1×10^5 HCC1954 and MCF-7 cells, respectively. Hybrid HER2+/– BC-MTS were produced by co-culturing 5×10^4 HCC1954 and MCF-7 cells, respectively. The BC-MTS were grown in ultra-low attachment 6 wells plates with DMEM/ F-12 supplemented with 10% FBS [37]. BC-MTS were used during the first 3 to 6 days of culture, when their diameter was between 50 to 200 μm. All cell cultures were grown in the dark at 37 °C/ 5% CO_2/ 95% air, using a CO_2 incubator MCO-18AIC(UV) (Sanyo Scientific, ILL, USA).

Aff and QD Conjugation

AffantiHER2-QD605 probe for HER2 detection and the negative control, Affneg-QD545 probe, were obtained by the irreversible conjugation between a reduced sulfhydryl group, present in the unique C-terminal cysteine of Aff, and the primary amine groups covering the QD surface, using the heterobifunctional cross-linker SMCC. QD (75 μl, 8 μM) were activated with 1.8 mM of SMCC dissolved in DMSO, during 1 h at room temperature (RT). Aff (100 μl, 1 mg/ ml) were reduced with 20 mM of DTT, during 1 h at RT, in order to obtain free sulfhydryl groups. Excess of DTT and SMCC in the reduced Aff and the activated QD suspensions, respectively, were removed using NAP-5 desalting columns and PBS-EDTA (2 mM, pH 7.2) as exchange buffer. The reduced Aff and the activated QD were mixed and incubated for 1 h at RT with constant gently shaking, to achieve the conjugation reaction. The conjugation was quenched by *β*-mercaptoethanol (110 μM). The resulting Aff-QD conjugates (probes) were purified using a Nap-10 desalting column and stored in PBS (pH 7.2) at 4 °C in the dark, and were used within the first 21 days after their production. The concentrations of AffantiHER2-QD605 and Affneg-QD545 were obtained from fluorescence standard curves of QD545 and QD605 (excited at 485 nm and emission recorded at 528 and 590 nm, respectively), using a multi-mode microplate Reader Synergy HT and a Take3 plate (BioTek Instruments, Inc., VT, USA). Fluorescence of SMCC-activated QD605 and QD545, and absorbance at 280 nm of reduced Affanti-HER2 and Affineg, were analyzed to obtain the concentration of both Aff and QD after the desalting process. The hydrodynamic size of Aff-QD probes was assessed by dynamic light scattering (DLS) using a Zeta sizer nano S (Malvern instruments, Worcestershire, UK) equipped with He-Ne Laser 633 nm. Aff-QD probes were filtered through a 0.22 μm filter before DLS analysis. The hydrodynamic size was obtained from the intensity size distribution parameter [38,39].

Flow Cytometry

To determine the affinity of conjugated Aff-QD probes, HCC1954 cells (2×10^5 cells) were incubated with increasing concentrations (0 to 40 nM) of either AffantiHER2-QD605 and Affneg-QD545 probes. MCF-7 cells were used as a negative control, to determine the HER2 specificity or non-specificity of both probes. After 1 h of incubation at 4 °C, cells were washed three times and resuspended in PBS, propidium iodide was added to exclude death cells, and suspensions were analyzed in a BD FACS Canto II (BD Biosciences, CA, USA). For data acquisition and analysis, we used the software FACSDiva (BD Biosciences, CA, USA) and FlowJo (Tree Star Inc., OR, USA), respectively. The median fluorescence intensity (MFI) was plotted as a function of probe concentration, and the dissociation constant (K_d) of AffantiHER2-QD605 was calculated with a one-specific binding equation using GraphPad Prism V. 2.0 (GraphPad Software Inc., CA, USA) [27].

Confocal Imaging

For specificity analysis of conjugated Aff-QD probes we used monolayer cultures of HER2+ and HER2– cells, at 60% of confluency. Cells were washed 3 times with PBS (pH 7.4), and gently shaken during 5 min, thereafter, they were fixed with 4% PFA for 10 min, washed again 3 times with PBS and blocked with 6% BSA during 2 h. Fixed cells were incubated with 10 nM of Aff-QD probes/ 6% BSA during 1 h, followed by 3 washes with PBS. To confirm the specificity of AffantiHER2-QD605 in HER2+ cells, an additional experiment was carried out where the cells were primarily incubated with a non-fluorescent unconjugated AffantiHER2-dim 250 μg/ ml/ 6% BSA, in order to block HER2. Thereafter, the cells were incubated with 10 nM of AffantiHER2-QD605/ 6% BSA. Finally, the cells nuclei were marked with 5 μM of DRAQ5. Confocal imaging was performed as described below.

For 3D HER2 analysis using Aff-QD probes, HER2+, HER2– and hybrid HER2+/– BC-MTS were obtained from 1 well and washed 3 times with PBS (pH 7.4) at 1500 rpm during 5 min, fixed with 4% PFA for 20 min, washed again 3 times with PBS and blocked with 6% BSA during 2 h. To permeabilize BC-MTS, they were incubated with 0.3% Triton X-100 (Triton) for 30 min before BSA blocking. Fixed BC-MTS were incubated with a mix (1:1) of 40 nM AffantiHER2-QD605 and Affneg-QD545 during 4 h with gentle shaking, and washed three times with PBS. Aff-QD probes incubation was carried out in the dark at RT. Fluorescence imaging of monolayer cultures was performed using a confocal microscope Leica TCS SP5 (Leica Microsystems, Wetzlar, DEU) equipped with two photomultipliers (PTM) for simultaneous data acquisition of both probes. QD545 and QD605 were excited with an Argon laser at 488 nm, and emission was collected between 520–560 and 590–640 nm, respectively. DRAQ5 was excited with a Helium/Neon laser at 633 nm and fluorescence emission was collected at 650–700 nm. Confocal images of fixed monolayer cultures were acquired in the XY scan mode (512 × 512 pixels) at 400 Hz, with a pinhole optimized for a resolution of ~1 μm in the Z distance, using a HCX PL APO 40×/ 1.3 NA oil immersion objective. Fluorescence signal of AffantiHER2-QD605 in HER2+ and HER2– monolayers cultures was analyzed by selecting two different regions of interest (ROI) of 80 × 80 μm, where cells nuclei were observed. Two additional ROIs of 30 × 30 μm devoid of cells, considered as background, were analyzed, and the mean value from both ROIs was subtracted from the AffantiHER2-QD605 signal. For confocal imaging of BC-MTS, simultaneous emission of both probes was collected with the same gain parameters (800 arbitrary units (A. U.)). Stacks of confocal sections (XY; 512 × 512 pixels), separated by 5 μm in the Z distance covering the whole thickness of the BC-MTS, starting at the bottom of the coverslip, were acquired in the XYZ scan mode at 400 Hz, with a section thickness of 5.5 μm, using an HC PL APO 20×/ 0.75 IMM objective. All confocal images were digitalized at a resolution of 8 bits.

Ratiometric Analysis of Breast Cancer Multicellular Tumor Spheroids Images

Assessment of the non-specific accumulation of Aff-QD probes within the complex 3D structure of HER2– BC-MTS was performed by RMA_{FI}, as proposed by Liu et al., 2009 [15], applying the formula: $FI_{AffantiHER2\text{-}QD605} / FI_{Affneg\text{-}QD545} = RMA_{FI}$. Where FI stands for

fluorescence intensity. On the one hand, $FI_{AffantiHER2\text{-}QD605}$ corresponds to the summation of two components: FI of the specific binding of AffantiHER2-QD605 to the HER2 receptor, plus FI of the non-specific accumulation of AffantiHER2-QD605. On the other hand, $FI_{Affneg\text{-}QD545}$, should be due only to its non-specific accumulation, because Affneg-QD545 does not recognize any epitope in mammal cells (Aff designed for Taq polymerase recognition [40]). Subtracting the non-specific fluorescence from the RMA_{FI} (see below) allowed us to assess HER2 specific detection within HER2+ BC-MTS (Z distance). HER2+ and HER2– BC-MTS with a diameter between 100–150 μm were selected for RMA_{FI} analysis. XY optical sections were processed using Fiji, the public domain software from ImageJ [41], which allowed us to select three ROI (12 × 12 μm) (Figure 4*C*), one in the center of the XY plane of the BC-MTS (labeled 1) and two more (labeled 2 and 3) positioned toward the BC-MTS periphery, with 8 μm of distance between them. Different color QD vary in their quantum yield and molar extinction coefficient (e.g. orange-red emission QD have higher brightness than green QD), therefore a scaling factor (SF) was required to normalize the FI of both probes for appropriate mathematical imaging processing [17,42]. The SF was assessed from the ratio between standard curves of the FI of QD605 and QD545 recorded with different concentrations of the probes (0, 10, 20, 40, 50, 80 nM of every QD) in a chamber at the stage of the confocal microscope used for cell imaging. With this procedure, a SF of 14.9 was obtained and it was also confirmed with the standard curves acquired in a microplate reader. Therefore, QD545 FI data in BC-MTS was post-processed by multiplying it by the SF, for figures presentation and for further analysis. Finally, RMA_{FI} was calculated using the mean values of FI of both Aff-QD probes obtained from each ROI along the Z distance recorded in the BC-MTS (100 μm).

For removal of the non-specific signal, due to Aff-QD probes accumulation within the BC-MTS, to allow specific HER2 signal quantification, from the signal of AffantiHER2-QD605 specifically bound to HER2, an ROI of 30 × 30 μm was selected in the optical sections acquired every 5 μm within the first 30 μm of the Z distance recorded. The $FI_{Affneg\text{-}QD545}$ was processed applying the SF of 14.9, and thereafter, FI of both Aff-QD probes were used to yield RMA_{FI}. Thereafter, we subtracted a unit from the RMA_{FI}. This is because a ratio equal to 1 is obtained when $FI_{AffantiHER2\text{-}QD605} = FI_{Affneg\text{-}QD545}$, therefore, we can assume that a ratio of 1 represents the non-specific probe accumulation. This operation (RMA_{FI}-*1*) was performed in every pixel contained within the ROI selected in the optical sections. Fluorescence in individual pixels might be affected by noise, due to random variations due to the low signal intensity collected by the PMT. This intrinsic noise might affect quantification of positive pixels for HER2, therefore, a threshold (T) was assessed, and subtracted from every pixel (RMA_{FI}-*1-T*). For this purpose, the mean FI of the pixels quantified after RMA_{FI}-*1* in the HER2– and HER2+ BC-MTS was obtained, and was fitted with Gaussian distribution functions, and the intersection of both functions was selected as T. Thereafter, pixels with positive values for FI in a confocal section were considered specific for HER2+, quantified and presented as HER2 density (%). The sum of HER2 density (%) for every optical section analyzed in the Z distance was reported as HER2 3D-density (%). Since the resultant values of RMA_{FI}-*1-T* are small, for illustration purposes, the values of every pixel showed in the images were achieved by multiplying RMA_{FI}-*1-T by* 30, to enhance their visibility. The mathematical processing was performed pixel-by-pixel in the optical sections (RMA_{FI}-*1,* RMA_{FI}-*1-T*, HER2 density (%) and HER2 3D-density (%)), and was automatized using MATLAB Software (The MathWorks, MA, USA).

Breast Cancer Multicellular Tumor Spheroids Immunohistochemistry

HER2 expression in HER2–, HER2+ and HER2+/– BC-MTS was analyzed by IHC by the pathology service of Hospital San José, Tecnologico de Monterrey, Mexico. Briefly, BC-MTS were fixed with PFA 4% during 20 min at RT, followed by three washes with PBS. The BC-MTS where extended on a slide positive charged for improved BC-MTS adhesion, and alcohol dehydration and immunostaining was performed using the automatized platform Benchmark GX (Ventana Medical Systems Inc., AZ, USA) with the Ultraview universal DAB detection IHQ kit and the Pathway anti-HER-2/neu (4B5) rabbit monoclonal primary AB. Counterstaining was made with hematoxylin. HER2 expression level was evaluated in the stained BC-MTS by a pathologist expert in BC, following the ASCO/CAP guidelines.

Statistical Analysis

Statistical comparison between groups was assessed with unpaired Student's t-test. and performed with Microsoft Excel (2016, WA, USA). A P value $< .05$ was considered significant. Data were presented as mean ± standard error of the mean (SEM). The number of individual experiments or total of replicates is represented by N.

Results

Aff-QD Probes Characterization: Size, Affinity and Specificity

Conjugation of Aff and QD was efficiently performed by the maleimide reaction, since both hybrid particles Aff-QD showed a significant increase in their hydrodynamic size; from 20.77 ± 0.34 to 30.43 ± 0.75 nm (N = 4) for QD545 and Affneg-QD545, respectively; and from 26.08 ± 0.17 to 30.69 ± 0.95 nm (N = 3/4) for QD605 and AffantiHER2-QD605, respectively ($P < .05$). Nevertheless, there was not significant size difference between AffantiHER2-QD605 and Affneg-QD545, $P > .05$). Since during the conjugation process, loss of reduced Aff and SMCC-activated QD could occur (due to retention in the column during the desalting step), and this could affect the expected Aff:QD ratio, we analyzed the Aff and QD total amount after the desalting step. We found that the Affanti-HER2 and Affneg amount was reduced by ~15 and ~10%, respectively (12.39 ± 1.56 nmole and 13.04 ± 1.59 nmole (N = 4), for AffantiHER2 and Affneg, respectively, compared with their respective Aff initial value of 14.5 nmole). The total amount of QD605 and QD545 was reduced by ~18 and 15%, respectively (0.49 ± 0.01 nmole and 0.51 ± 0.0 nmole (N = 4), for QD605 and QD545, respectively, compared with their respective QD initial value of 0.6 nmole). This resulted in a Aff:QD ratio of 25.3 and 25.6 for AffantiHER2-QD605 and Affneg-QD545, respectively. The above results suggest that both probes should have comparable penetrability within BC-MTS, and therefore should satisfy the condition of similar non-specific probe accumulation for correct RMA_{FI} performance.

Binding affinity and specificity of the Aff could be altered by the chemical reaction involved in the conjugation process. The reported K_d for unconjugated AffantiHER2 was ~0.032 nM [43], however, we found that upon conjugation with the QD605, the AffantiHER2 affinity, obtained from a saturation binding curve in HER2+ cells

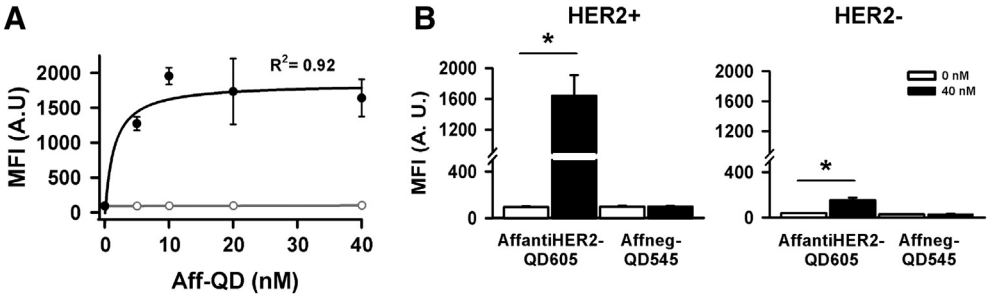

Figure 1. Affinity binding and specificity of Aff-QD probes assessed by flow cytometry. (A) Saturation assay, pooled data of the median fluorescence intensity (MFI) signal in HER2+ cells (HCC1954) incubated with increasing concentrations of AffantiHER2-QD605 (black circles) and Affneg-QD545 (white circles). AffantiHER2-QD605 MFI was fitted with a one-site specific binding equation (black line). (B) Pooled data of MFI in HER2+ cells incubated with AffantiHER2-QD605 and Affneg-QD545 at 0 and 40 nM (left panel). Pooled data of MCF-7 cells (HER2–) incubated with AffantiHER2-QD605 and Affneg-QD545 (right panel). A. U., arbitrary units.

(Figure 1*A*), decreased (1.10 ± 0.38 nM, N = 3 independent experiments). Nevertheless, the K_d of the conjugated probe remained within the nM range, therefore, it is still considered high affinity. Probe specificity assessed by flow cytometry analysis showed that HER2+ cells presented significant (~17.2-fold) increase in MFI upon incubation with AffantiHER2-QD605 (40 nM), compared with cells without incubation (95.4 ± 6.4 A. U. and 1641.3 ± 265.4 A. U., for 0 and 40 nM, respectively. N = 4, $P < .05$) (Figure 1*B*, left panel). In the case of HER2– cells, a significant increase in MFI was also found, however, this was only ~3.8-fold higher when incubated with 40 nM of AffantiHER2-QD605, compared with non-incubated cells (40.0 ± 0.9 A. U. and 151.4 ± 24.6 A. U., for 0 and 40 nM, respectively. N = 4, $P < .05$) (Figure 1*B*, right panel). Despite that we observed an increase in MFI in HER2– upon incubation with 40 nM of AffantiHER2-QD605, this increase was much smaller than that observed for HER2+ cells, even when it was compared with the MFI increase observed with a lower AffantiHER2-QD605 concentration (5 nM) in HER2+ cells (~13 fold higher than without incubation, obtained from the saturation curve). There was not difference in the MFI acquired in HER2+ and HER2– cells incubated with Affneg-QD545, compared with cells without incubation with the probe (HER2+: 98.9 ± 6.2 A. U. and 99.6 ± 4.4 A. U.; and HER2–: 28.3 ± 1.1 A. U. and 31.0 ± 1.8 A. U., for 0 and 40 nM, respectively. N = 3/4, $P > .05$) (Figure 1*B*).

The specificity of AffantiHER2-QD605 and lack of specificity of Affneg-QD545 probes were also assessed by confocal microscopy in

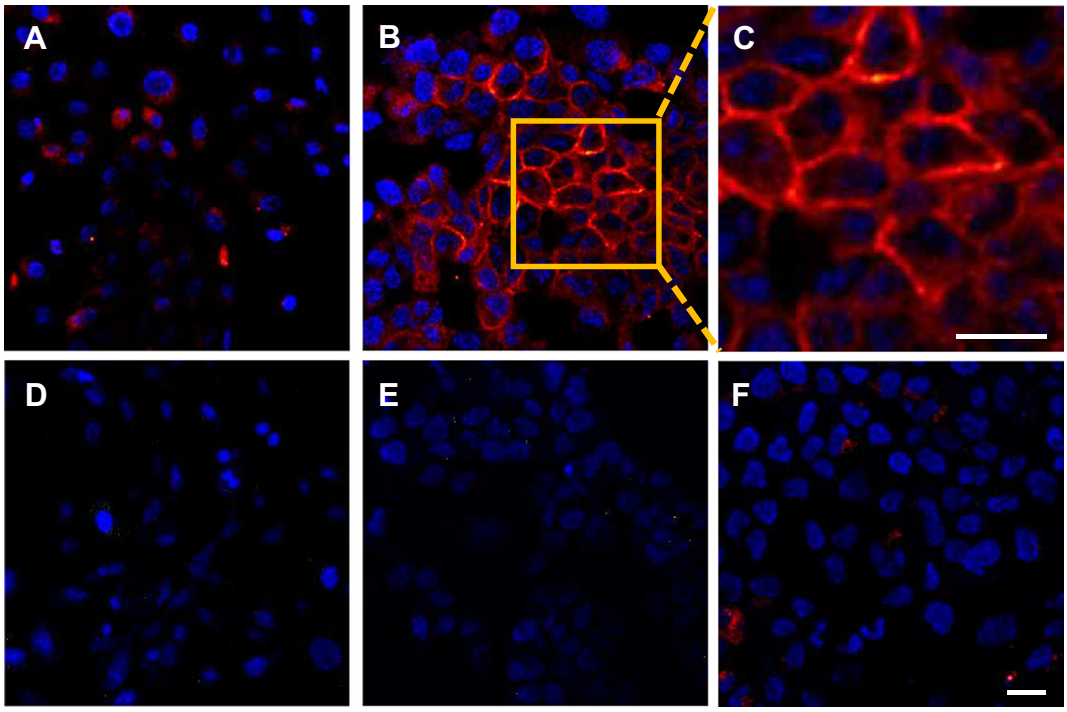

Figure 2. Confocal images of monolayer BC cells cultures incubated with Aff-QD probes.(A) HER2– cells (MCF-7) incubated with AffantiHER2-QD605 (red signal). Scarce fluorescence signal is observed in HER2– cells. (B) HER2+ cells (HCC1954) incubated with AffantiHER2-QD605. (C) Magnification of the ROI indicated in the image of HCC1954 cells with AffantiHER2-QD605 in panel B to highlight the specific pattern of HER2 distribution. (D) HER2– cells incubated with Affneg-QD545. (E) HER2+ cells incubated with Affneg-QD545. (F) HER2+ cells were blocked with AffantiHER2-dim, and thereafter incubated with AffantiHER2-QD605**.** Draq5 (blue signal) is observed in the nucleus in all panels. Scaling bars represent 20 μm.

monolayer cell cultures. Fluorescence signal of the AffantiHER2-QD605 probe was mostly located, in a specific pattern, at the level of the plasma membrane of HER2+ cells (Figure 2*B* and *C*). This pattern of HER2 detection, around the cell, obtained with the Aff-QD probe, is similar to that observed with AB conjugated with QD [17]. In this study, we used the AffantiHER2-dim (dimeric variant of ZHER2:477 Aff [43,44]) at a concentration of 250 μg/ml, which is 50-fold higher compared to the concentration used to detect HER2 in a similar overexpressed HER2 cell line (5 μg/ ml) in monolayer culture [44]. Using this high AffantiHER2-dim concentration, we assured complete HER2 blocking in HCC1954 cells, and since no signal was observed after incubation with conjugated AffantiHER2-QD605 (based in the monomeric modified variant of ZHER2:477 Aff) we confirmed the specificity of this conjugated probe (Figure 2*F*). In HER2– cells, scarce and non-organized fluorescence signal was observed, mostly in the cytosol (Figure 2*A*), and, it was on average only ~15% of that observed in HER2+ cells (31.1 ± 2.4 A. U. and 4.8 ± 0.4 A. U. for HER2+ and HER2–. N = 5/ 4 experiments, 26/ 22 images analyzed. $P < .05$). These results confirmed that the MFI and confocal fluorescence signals of AffantiHER2-QD605 in HER2+ cells were due to specific HER2 recognition. In the case of Affneg-QD545, the confocal fluorescence signal was negligible in HER2– cells (Figure 2*D*) and in HER2+ cells (Figure 2*E*), since it did not bind to any epitope, and the probe was completely washed off, supporting the lack of specific binding of this probe to HER2, and confirming the flow cytometry results. Therefore, Affneg-QD545 could be used as a negative control.

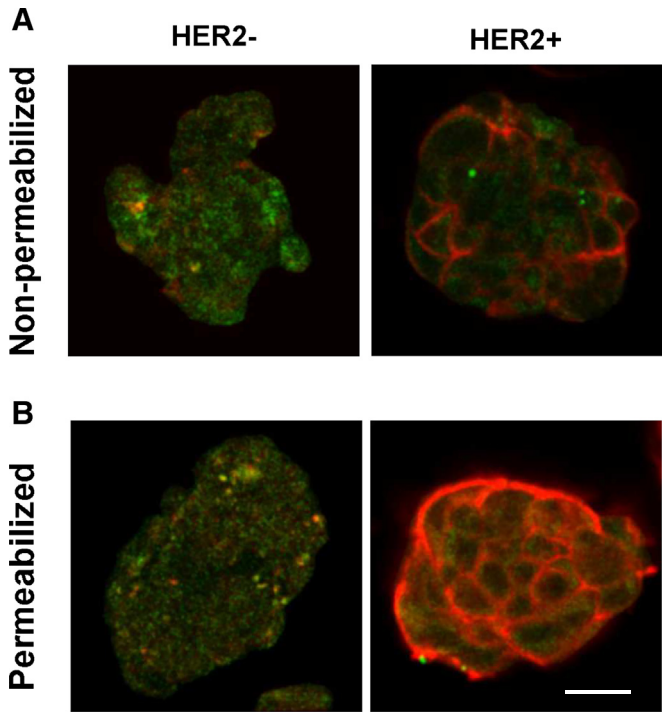

Figure 3. Multiplexed confocal images of breast cancer multicellular tumor spheroids incubated with two Aff-QD probes.(A) Merged image of signal of AffantiHER2-QD605 (red) and Affneg-QD545 (green) observed in optical sections acquired at a depth of 25 μm within a HER2– BC-MTS (Notice the non-specific accumulation of both Aff-QD probes) and HER2+ (intense AffantiHER2-QD605 due to HER2 recognition, and non-specific accumulation of both Aff-QD probes) non-permeabilized BC-MTS. (B) Similar image presentation, as in panel A, for Triton-permeabilized BC-MTS. Scaling bar represents 30 μm.

HER2 Detection Within Breast Cancer Multicellular Tumor Spheroids

The previous studies were done in suspended individual cells and monolayers, therefore, few diffusion barriers complicate HER2 detection with the specific probes. Nevertheless, poor probe penetration and wash off process could complicate HER2 detection within thick biological samples due to diffusional barriers created by cell junctions and extracellular matrix components. Therefore, as a 3D model of BC, we used BC-MTS, and assessed the non-specific signal accumulation and the maximal Z distance at which HER2 could be specifically detected. For this purpose, HER2+ HER2– and BC-MTS (non-permeabilized and Triton-permeabilized) were incubated with a 1:1 mixture of Aff-QD probes. Figure 3*A* shows representative optical sections, at 25 μm in the Z distance within non-permeabilized HER2– and HER2+ BC-MTS, of the spatial distribution of the fluorescence signals for both, AffantiHER2-QD605 and Affneg-QD545. Figure 3*B* shows representative Triton-permeabilized HER2– and HER2+ BC-MTS, incubated with the Aff-QD probes, as indicated above. It is clear from those images that diffuse fluorescence signal of both probes was observed in HER2– BC-MTS (merging of red and green signals, from AffantiHER2-QD605 and Affneg-QD545, respectively), where fluorescence could be attributed to non-specific accumulation. Interestingly, diffuse fluorescence of both probes was also observed in HER2+ BC-MTS, although stronger signal of AffantiHER2-QD605 was clearly present surrounding the cells, which should be related with the specific HER2 detection in the cell membranes within the BC-MTS.

Furthermore, to assess whether Affneg-QD545 and Affanti-HER2-QD605 are non-specifically accumulated within the BC-MTS, we performed RMA_{FI} in HER2– BC-MTS, where most of the fluorescent signal should correspond to non-specific accumulation of both probes. RMA_{FI} was processed from the mean FI of an ROI localized in the center of BC-MTS (in the XY plane; ROI 1, Figure 4*C*). In HER2– BC-MTS, RMA_{FI} yielded values close to 1 throughout the whole Z distance recorded (100 μm), in non-permeabilized and permeabilized BC-MTS (Pooled data are shown in Figure 4*A* and *B*, black circles). Therefore, most of the signal of AffantiHER2-QD605 observed in the HER2– BC-MTS should be similar to that of the Affneg-QD545 probe (if AffantiHER2-QD605 = Affneg-QD545, then the $RMA_{FI} = 1$). Therefore, based on these results, we assumed that both probes accumulated in similar way within the BC-MTS, supporting our RMA_{FI} analysis. On the other hand, in HER2+ BC-MTS we found significantly higher RMA_{FI} values than those in HER2– BC-MTS, closely correlating with the higher FI observed of AffantiHER2-QD605 surrounding the cells. Nevertheless, in the non-permeabilized HER2+ BC-MTS, those higher values in ROI 1 only were found in the most superficial optical sections (<30 μm and at >70 μm; Figure 4*A*, white circles). Furthermore, in the most internal optical sections (from 35 to 65 μm of Z distance) no significant difference was found between the two types of BC-MTS, suggesting limited probe penetration. Similar trend in RMA_{FI} distribution along the thickness of the BC-MTS was also observed when we assessed two additional ROIs, located in eccentric positions (Supplementary Figure 1A). Nevertheless, as expected, since those ROIs were closer

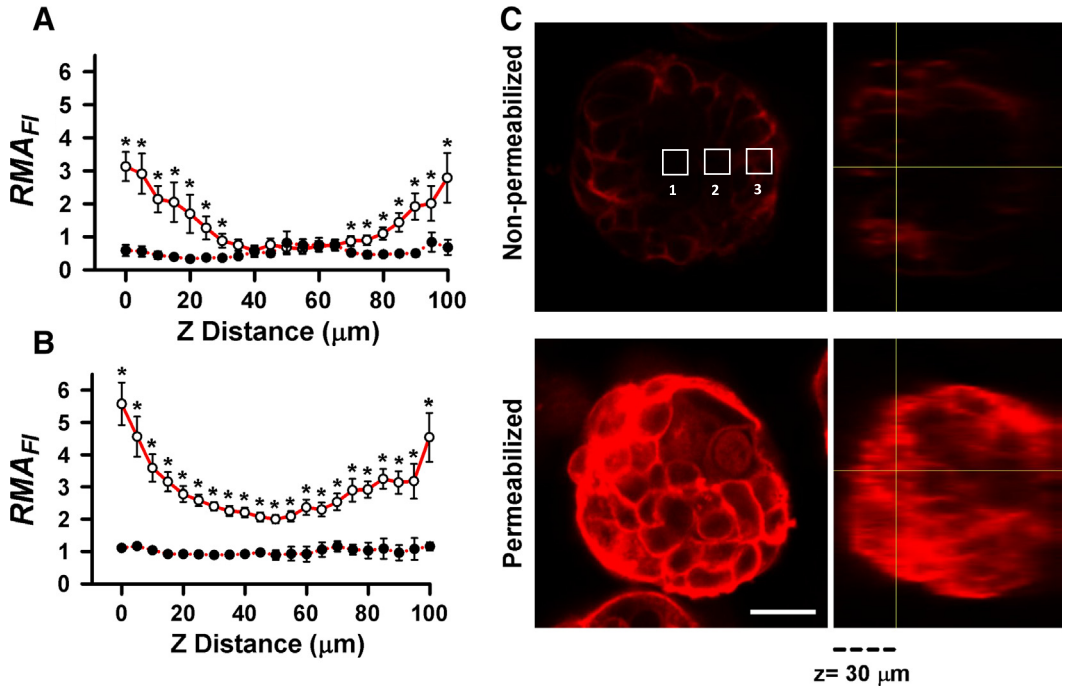

Figure 4. HER2 detection within Z distance of non-permeabilized and Triton-permeabilized HER2+ and HER2– breast cancer multicellular tumor spheroids.(A) Pooled data of the $FI_{AffantiHER2\text{-}QD605}$ /$FI_{Affneg\text{-}QD545}$ (RMA_{FI}) analyzed in a region of interest (ROI) positioned in the center of BC-MTS in the XY plane (ROI labeled 1 in panel C) of a stack of optical sections separated by 5 μm in the Z distance. Data were obtained from non-permeabilized HER2+ (white circles) and HER2– (black circles) BC-MTS (N = 4 experiments/ 26 BC-MTS for HER2+ and 5/ 25 for HER2–), $P < .05$. (B) Similar analysis as in panel A, in both types of BC-MTS permeabilized with Triton (see methods) (N = 4 experiments/ 33 BC-MTS for HER2+ and 5/ 36 for HER2–), $P < .05$. (C) Representative optical sections acquired at a depth of 50 μm within the non-permeabilized and permeabilized BC-MTS (left panels), and their respective orthogonal view (right panels). AffantiHER2-QD605 signal is observed in red. Scaling bar represents 30 μm and z represents Z distance.

to the BC-MTS surface, higher RMA_{FI} values in more internal optical sections were observed, presumably because probe penetration was better in those regions. These results show that Aff-QD probes presented limited penetration within the center of non-permeabilized BC-MTS, and this could be better appreciated in the orthogonal view of a representative non-permeabilized HER2+ BC-MTS in Figure 4*C* (upper panel). Therefore, RMA_{FI} only allowed specific HER2 detection up to ~30 μm of depth in non-permeabilized BC-MTS. In contrast, in permeabilized BC-MTS (Figure 4*B*), the RMA_{FI} of ROI 1 in the HER2+ group was significantly higher throughout the whole Z distance analyzed, compared with the HER2– group. Similar to non-permeabilized BC-MTS, the optical sections in the most internal layers (center) of the permeabilized HER2+ BC-MTS presented lower RMA_{FI}, nevertheless, the RMA_{FI} values were always at least two-fold higher. In the orthogonal views of HER2+, non-permeabilized and Triton-permeabilized BC-MTS (Figure 4*C*), we could notice that in deeper regions (beyond ~70 μm), reduced FI is observed, which could be related to the intrinsic optical limits of confocal microscopy. Nevertheless, the results presented in Figure 4*B* demonstrate that Aff-QD probes have better penetration within permeabilized BC-MTS, and most important, HER2 could be specifically detected within the whole Z distance recorded (Figure 4*C*, lower panel). Similar pattern of HER2 detection of HER2+ permeabilized BC-MTS was observed in two additional eccentric ROIs (Supplementary Figure 1B).

3D Quantification of HER2 in Breast Cancer Multicellular Tumor Spheroids

Since both probes shared similar non-specific accumulation, we explored the removal of the non-specific signal, pixel-by-pixel using RMA_{FI}*-1*, in non-permeabilized and permeabilized BC-MTS. In the first 7 optical sections, where HER2 was clearly detected in both groups (30 μm of depth; see Figure 4*A-B*), a central region (XY plane; 30 × 30 μm), was subjected to RMA_{FI}*-1*.

To accurately yield HER2 3D-density, avoiding false positive due to noise fluctuations in pixels close to a ratio of 1, thresholding of RMA_{FI}*-1* was required, as described below. We found HER2 3D-density of 18.7 ± 2.5% and 39.8 ± 2.1% (N = 5 experiments, 22/ 35 BC-MTS) for HER2– non-permeabilized and Triton-permeabilized BC-MTS, respectively. Nevertheless, HER2 3D-density was significantly higher in both, the HER2+ non-permeabilized and Triton-permeabilized BC-MTS, compared with HER2– BC-MTS, under similar conditions (33.8 ± 5.1% and 72.8 ± 1.7% respectively. N = 4 experiments, 22/ 33 BC-MTS. $P < .05$). For the non-permeabilized BC-MTS, we found that those HER2+ pixels quantified as a HER2 3D-density in HER2+ BC-MTS had a mean FI of ~1.5 times higher than that of HER2– BC-MTS (1.49 ± 0.11 and 0.99 ± 0.06, for HER2+ and HER2–, respectively. $P < .05$). While in the permeabilized BC-MTS the difference was significantly higher, with a mean value ~3.2 times higher in HER2+ BC-MTS compared with HER2– BC-MTS (2.7 ± 0.22 and 0.85 ± 0.04, for HER2+ and HER2–, respectively. $P < .05$). Since such a significant

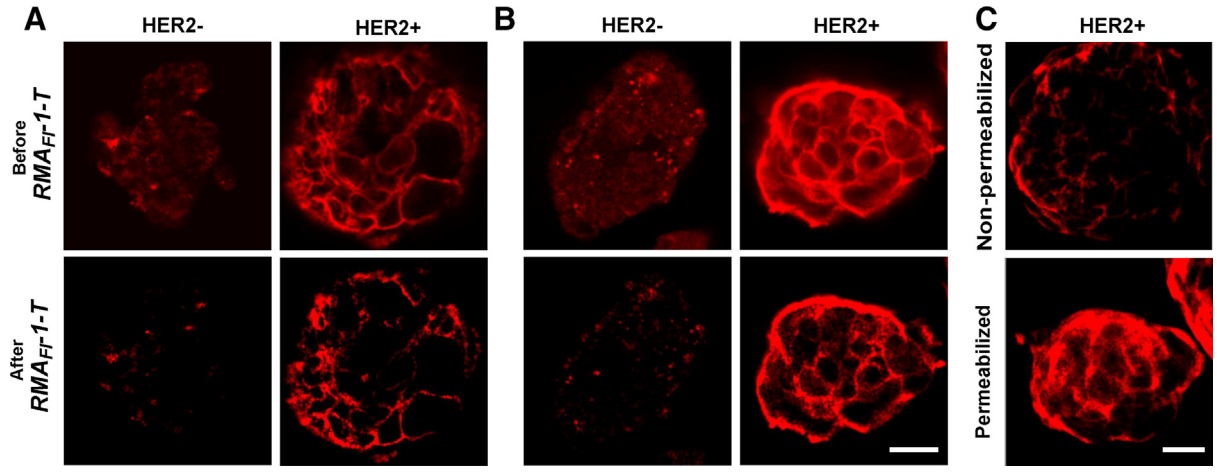

Figure 5. Mathematical removal of the signal corresponding to non-specific accumulation of Aff-QD probes within breast cancer multicellular tumor spheroids.(A) Optical sections recorded at a depth of 25 μm within non-permeabilized HER2– and HER2+ BC-MTS. AffantiHER2-QD605 signal (red) is observed in the same BC-MTS before $FI_{AffantiHER2\text{-}QD605}$ /$FI_{Affneg\text{-}QD545}$–*1-T* (*RMA$_{FI}$-1-T*) (upper panels) and after *RMA$_{FI}$-1-T* (lower panels). (B) Similar data presentation, as in panel A, for Triton-permeabilized BC-MTS, before and after *RMA$_{FI}$-1-T*. (C) 3D projection of AffantiHER2-QD605 signal after *RMA$_{FI}$-1-T* in a non-permeabilized (upper panel) and in a Triton-permeabilized HER2 + BC-MTS (lower panel). Scaling bars represent 30 μm for all panels.

difference in mean FI values, after *RMA$_{FI}$-1*, was found between the HER2– and HER2+ groups, the intersection of Gaussian distribution fittings of both groups allowed us to objectively determine the value of T. Thresholding (*RMA$_{FI}$-1-T*) was performed in every pixel contained in the optical sections analyzed, and the non-specific fluorescence was efficiently removed.

After *RMA$_{FI}$-1-T*, the remaining signal in HER2+ BC-MTS was specifically localized surrounding the cell, at the level of the cell

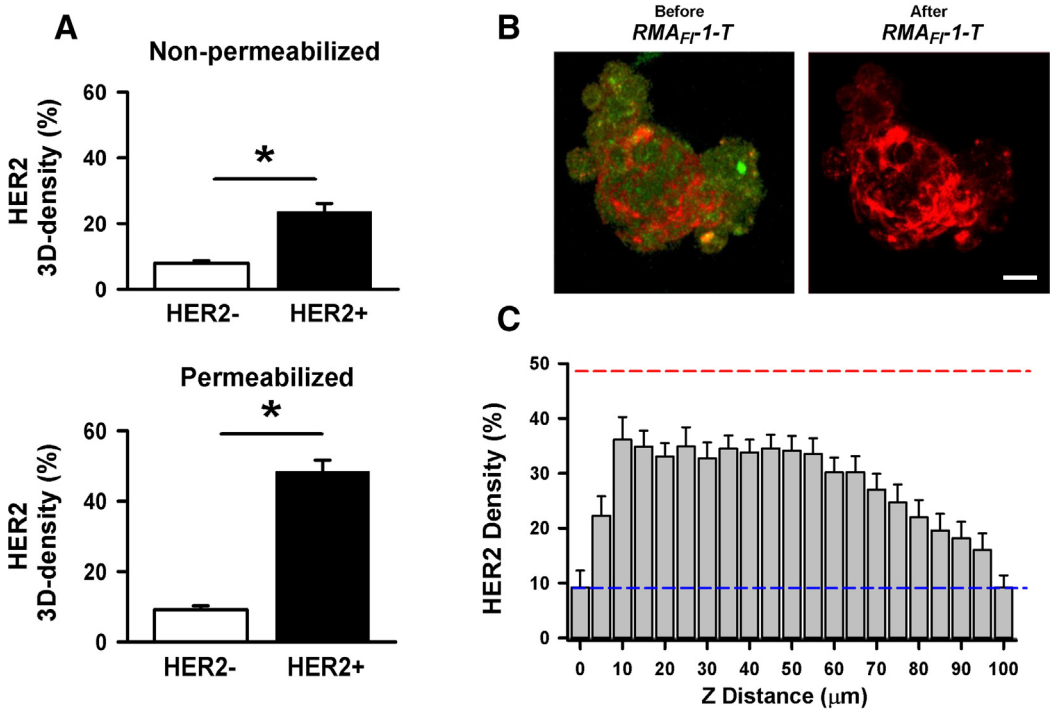

Figure 6. HER2 quantification in breast cancer multicellular tumor spheroids. (A) Pooled data of the percent of HER2+ signal (HER2 3D-density) (see methods) quantified after $FI_{AffantiHER2\text{-}QD605}$ /$FI_{Affneg\text{-}QD545}$–*1-T* (*RMA$_{FI}$-1-T*) in non-permeabilized HER2+ and HER2– BC-MTS (upper panel). Pooled data of HER2 3D-density in Triton-permeabilized HER2+ and HER2– BC-MTS (lower panel). (B) AffantiHER2-QD605 signal (red) and Affneg-QD545 signal (green) observed in a 3D projection of a permeabilized hybrid HER2+/– BC-MTS (see methods), before (Left) and after (Right) *RMA$_{FI}$-1-T*. Scaling bar represents 30 μm. (C) Pooled data of the percent of HER2+ signal (HER2 density) quantified after *RMA$_{FI}$-1-T* from each optical section acquired every 5 μm in the Z distance within permeabilized hybrid HER2+/– BC-MTS. Dashed lines represent the HER2 3D-density assessed in permeabilized HER2+ (red) and HER2– (blue) BC-MTS.

membrane, in both the non-permeabilized and permeabilized groups (Figure 5*A* and *B*, lower panels, right). Nevertheless, higher signal of *RMA_{FI}-1-T* was observed in the permeabilized group along the complete Z distance recorded (Figure 5*C*, lower panel and Supplementary Figure 2), while in the non-permeabilized group the signal was reduced in the internal regions of the BC-MTS (Figure 5*C*, upper panel). Importantly, in both groups of HER2– BC-MTS the non-specific signal was almost eliminated upon *RMA_{FI}-1-T*, and sharper images were obtained (Figure 5*A* and *B*, lower panels, left). These results demonstrate that false positive signals of Aff-QD probes, due to the non-specific accumulation, could be efficiently removed by *RMA_{FI}-1-T*. The magnitude of HER2 3D-density was re-calculated considering the positive HER2 pixels obtained after *RMA_{FI}-1-T*, and we found that HER2 3D-density was ~3 times higher in non-permeabilized HER2+ BC-MTS compared with HER2– (23.5 ± 2.6% and 8.0 ± 0.7% for HER2+ and HER2–, respectively. $P < .05$) (Figure 6*A*, upper panel). Furthermore, in permeabilized BC-MTS a significantly higher value of ~5 times HER2 density was observed in the HER2+ group (48.3 ± 3.3% and 9.2 ± 1.1% for HER2+ and HER2–, respectively. $P < .05$) (Figure 6*A*, lower panel). These results demonstrate that HER2 could be efficiently assessed after *RMA_{FI}-1-T* in BC-MTS, as a model of 3D cancer culture, mimicking thick tumor tissue samples. Furthermore, in permeabilized HER2+ BC-MTS, the HER2 3D-density was ~2 times higher ($P < .05$) than in non-permeabilized HER2+ BC-MTS. These results demonstrate that diffusion barriers even in those regions closer to the BC-MTS surface (since the HER2 quantification was performed in the first 30 μm recorded), could affect HER2 detection and quantification in relatively intact biological samples. Nevertheless, more efficient HER2 detection and quantification were assessed in Triton-permeabilized BC-MTS, which removed the diffusion barriers, allowing efficient detection within the whole thickness of the sample.

All the experiments presented so far, were performed in cell cultures of independent cells lines, where the pattern of protein expression (e.g., HER2) should be relatively homogeneous among the cells. Nevertheless, tumors normally show high level of heterogeneity, therefore, to mimic this heterogeneity in vitro, we created a model of hybrid HER2+/– BC-MTS, by co-culturing both cell lines (MCF-7 and HCC1954). Growth of HER2+/– resulted in BC-MTS with more irregular shapes, where some BC-MTS showed spheroid form, while others were more elongated, however, they did not disaggregate during the wash steps or when mechanical force was applied with a pipette tip. Triton-permeabilized HER2+/– BC-MTS were incubated with AffantiHER2-QD605 and Affneg-QD545, (1:1). Combined signal of AffantiHER2-QD605 and Affneg-QD545, presented irregular distribution, in the non-processed sample (Figure 6*B*, left panel), with some regions richer in combined signals than others. These large regions of non-specific signal (associated to clusters of HER2– cells) were observed along the complete Z distance recorded (Supplementary Figure 3) and are consistent with heterogeneous growth of the co-culture. Nevertheless, more intense fluorescence, corresponding with the specific binding of AffantiHER2-QD605, were observed in some regions (Figure 6*B*, left panel) and after mathematical processing (*RMA_{FI}-1-T*), the broadly distributed, non-specific signal, was efficiently removed and clusters of HER2+ cells where identified within the hybrid BC-MTS (Figure 6*B*, right panel). In each of the optical sections, acquired between 10 to 70 μm of the Z distance, HER2 density was calculated, yielding values between ~30 to ~40% (Figure 6*C*). Nevertheless, from 70 to 100 μm (further away from the coverslip surface), we observed a decrease in the magnitude of HER2 density, which should be related to the maximal imaging depth of confocal microscopy. Therefore, a more reliable HER2 3D-density was calculated considering only the values for the optical sections ≤70 μm of depth. The resulting magnitude of HER2 3D-density was 30.8 ± 2.1% (4 experiments/ 18 BC-MTS) in the permeabilized HER2+/– BC-MTS, which corresponds to slightly over half (~64%) of the HER2 3D-density found in permeabilized HER2+ BC-MTS. These results confirmed that *RMA_{FI}-1-T*, could efficiently remove non-specific signal and allowed objective quantification of HER2 3D-density in a hybrid 3D model of BC, which resemble the biomarker heterogeneity typically found in tumors growth.

In order to confirm, the results of the pattern of HER2 3D distribution found in the different BC-MTS using Aff-QD probes, conventional IHC analysis was performed in these 3D samples. MCF-7 BC-MTS showed some low staining in the cytoplasm, however, specific membrane staining was not observed (Figure 7*A*), and were classified as HER2– with an IHC score of 0. In HCC1954 BC-MTS, intense staining was observed at the level of the membrane but also in the cytosol (Figure 7*B*), which could be attributed to the processing of the 3D sample and imaging, which is not confocal and collects light from the whole thickness of the sample. These BC-MTS were classified as HER2+, with an IHC score of 3+. On the other hand, hybrid BC-MTS showed a heterogeneous distribution of clusters with intense staining, identified as HER2+, and other clusters with no membrane staining identified as HER2– (Figure 7*C*). Nevertheless, since in the hybrid BC-MTS, more than the 10% of the cells observed were identified as HER2+, according to the ASCO/CAP guideline [9], these were classified as HER2+, with an IHC score of 3+. These results confirmed that these BC-MTS could be considered as appropriate 3D models of different HER2 overexpression levels (HER2–, HER2+ and hybrid HER2+/–), which is in agreement with the HER2 3D-density assessed with Aff-QD probes and the *RMA_{FI}-1-T*.

Discussion

In this study, using simultaneously two Aff-QD probes, *RMA_{FI}* analysis and thresholding, objective and specific HER2 detection was assessed in a 3D model of BC. Preparation of Aff-QD probes, with retention of their high affinity (K_d ~1.1 nM) and specificity, was efficiently achieved by conjugation of commercially available Aff and QD, by a maleimide reaction, typically applied for AB-fluorophore and AB-QD conjugation [17,45,46]. The K_d of the conjugated AffantiHER2-QD605 was close to that of AffantiHER2 conjugated with a conventional fluorophore (DyLight) (K_d ~3.7 nM) [27]. Although, both K_d values are higher than the reported for the anti-HER2 monoclonal AB Trastuzumab (Herceptin; K_d of ~0.09 nM) [47], they are within the range of other anti-HER2 monoclonal AB (~0.09 to 26 nM) [47,48]. Nevertheless, a decrease in affinity of the conjugated probe does not necessarily translates to lower detection efficiency of HER2 in a 3D tissue. In *in vivo* studies, it has been documented that higher affinity of monoclonal AB could reduce tumor intake of the probe, which is related with a decrease of the free AB available to diffuse into the tumor, known as the model of "binding site barrier", or due to antigen expression and internalization of bound probe [47,49]. For example, Trastuzumab had significantly lower penetration, compared with a lower affinity AB (K_d of ~23 nM

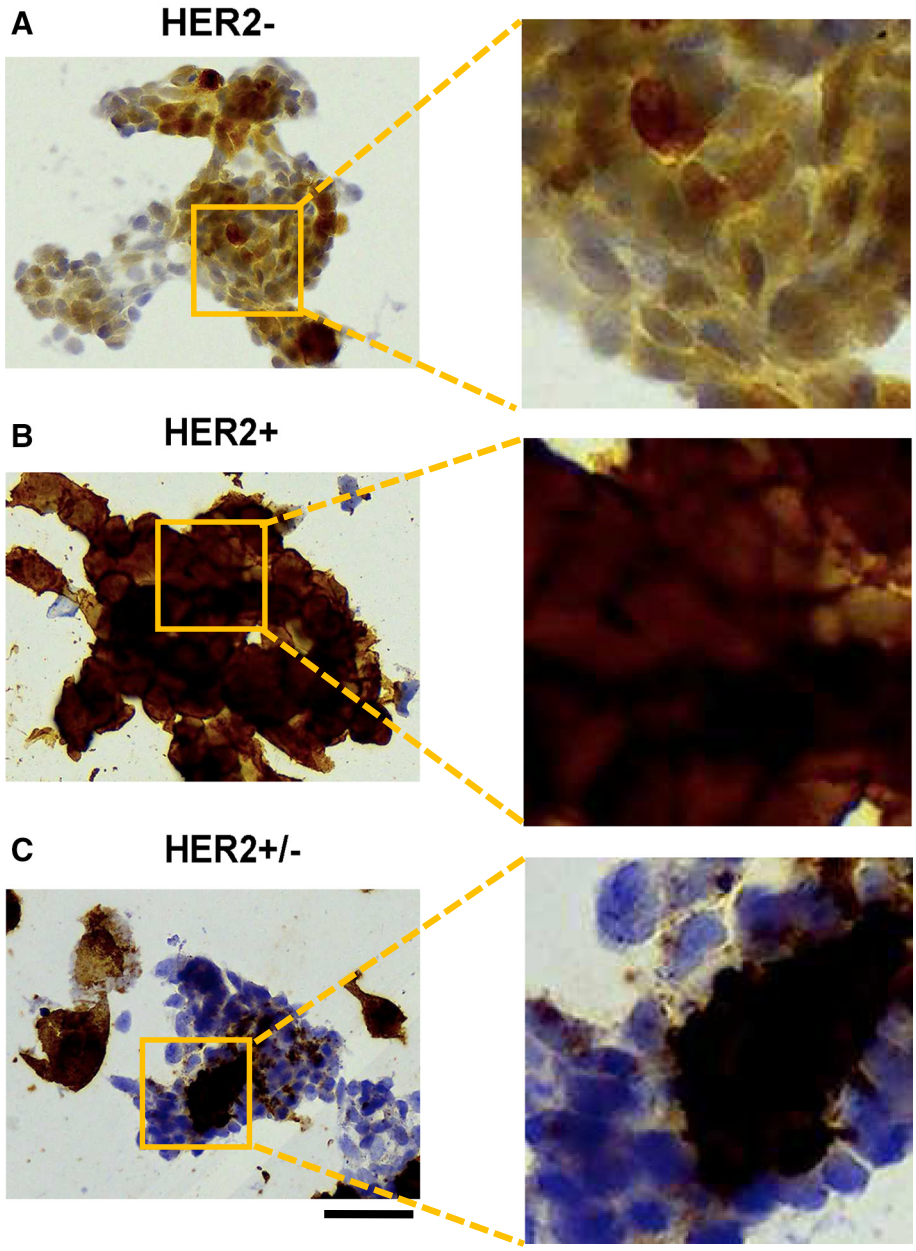

Figure 7. Immunohistochemistry of breast cancer multicellular tumor spheroids with different HER2 expression.Expression of HER2 evaluated by IHC in BC-MTS with different HER2 expression (A-C). (A) HER2 overexpressed (HCC1954). (B) HER2 basal-expressed (MCF-7). (C) Hybrid HCC1954/ MCF-7 BC-MTS. Right images: Magnification of the ROI indicated in the main images on the left, to highlight the expression pattern of HER2 in the respective samples. Scaling bar represents 50 μm.

[47]). Furthermore, in our study, the conjugated AffantiHER2-QD605 probe with a K_d of ~1.1 nM yielded appropriate penetration in Triton-permeabilized BC-MTS, and allowed us to perform 3D reconstructions of HER2 distribution up to a Z distance of ~70 µm.

In this study, we used BC-MTS, as a 3D model of BC growth. MTS, are cell aggregates which grow forming spheroid structures, where their intercellular interactions and protein expression profiles resemble those observed in *ex vivo* or *in vivo* tissue samples [30,37]. For 3D imaging of molecular target detection within BC-MTS, the probe must have appropriate penetration in the inner layers of cells within the sample. However, diffusional barriers could prevent adequate penetration, and also limit appropriate wash off process of unbound probe, which causes that a fraction of the probe remains accumulated within the sample, in a non-specific manner, and hence, leading to false positive signal, complicating quantification accuracy. Non-specific probe accumulation has been a particular problem for molecular target detection in studies *in vivo* [16,50], in processed tissue samples and in 3D cancer models [15,38]. In a multiplexed study of 3 molecular targets, performed by Park *et al.* (2014), in a mouse thick tissue model of colon cancer, the anti-carcinoembryonic antigen AB-QD probe yielded false positive signal, comparable to that of the non-specific signal obtained with an isotype control IgG-QD. False positive detection was confirmed by histopathology, and attributed to non-specific accumulation of the AB-QD probe [38]. In order to reduce the effect of non-specific probe accumulation within BC-MTS, in this study, we took advantage of the multiplexing

capacity of QD and confocal microscopy to simultaneous record two Aff-QD probes; one HER2 specific (AffantiHER2-QD605) and the second as negative control (Affneg-QD545), within HER2–, HER2+ and hybrid HER2+/– BC-MTS. Mathematical post-acquisition processing (RMA_{FI}-*1-T*) allowed us to remove the non-specific probe accumulation and uncover the specific HER2 distribution pattern within whole BC-MTS.

Since similar fluorescence pattern of AffantiHER2-QD605 and Affneg-QD545 was observed along the whole depth of permeabilized and non-permeabilized MCF-7 BC-MTS (Figure 4*A* and *B*), which have basal expression of HER2 [17,33,34], and was confirmed by IHC analysis as HER2– (Figure 7*A*), classified according to the pathologist as 0, although in various publications is recognized as 0 or 1+ [33,51], we demonstrated that both probes are non-specifically accumulated in a similar way within a relatively thick sample, validating our RMA_{FI} processing method. In contrast, in HCC1954 BC-MTS, where there is a well-documented HER2 overexpression [31,32], the AffantiHER2-QD605 yielded higher signal, with a distinctive spatial pattern (Figure 3, right panel), than that of the Affneg-QD545, and with RMA_{FI} values >1 (Figure 4*A* and *B*). Therefore, only a small fraction of AffantiHER2-QD605 signal in the HER2+ BC-MTS (similar to the Affneg-QD545 signal) is caused by non-specific probe accumulation, while the larger fraction, highly localized at the level of the cell membrane, corresponds to specific HER2 recognition by the AffantiHER2-QD605. Both commercial QD used in this study present the same functionalization in the surface (amino-PEG), and the two Aff used have similar molecular composition and structure (changes in only 11 amino acids of the Affneg scaffold [40]). Both conjugated Aff-QD were achieved with a similar reaction ratio (~25:1), and the resulting final size for both was ~30 nm. Therefore, it was expected that both probes presented similar non-specific accumulation patterns, when used at the same concentration. Furthermore, since Aff affinity and specificity were retained, AffantiHER2-QD605 presented different accumulation within HER2+ BC-MTS, due to specific molecular target recognition.

RMA_{FI} analysis demonstrated that HER2 detection was not properly achieved in the inner central layers of non-permeabilized HER2+ BC-MTS, which represents ~1/3 of the average thickness of the BC-MTS analyzed (~120 μm) (Figure 4*A* and *C*, upper panel). Nevertheless, improved HER2 detection, within the whole BC-MTS Z distance analyzed was achieved using Triton (Figure 4*C*, lower panel), a non-ionic surfactant typically used for plasma membrane permeabilization of individual cells, 2D or 3D cultures [52–54]. Despite that Aff-QD are larger than AB conjugated with conventional fluorophores, they displayed similar penetration in Triton-permeabilized BC-MTS, when compared with secondary AB-fluorophore probes used for detection of primary AB bound to other molecular targets in permeabilized spheroids, however, in that study 3D detection required an extended period of time (4 days) [53]. As expected, in HER2– Triton-permeabilized BC-MTS an increase in the fluorescence signal of Affneg-QD545, along the full BC-MTS thickness, was also observed, which was related to the non-specific accumulation of the probe (Figure 3*B*). The signal of the negative probe was essential during the post-acquisition image processing, for which we developed an automatized algorithm, since it allowed us to quantify specific HER2 signal (see below).

When working with 3D biological samples, and specific signals need to be resolved and quantified in all the 2D sections within the thickness of the sample, then the non-specific fluorescence signal due to accumulation within the sample represents a problem. In order to mathematically remove the signal of non-specifically accumulated probes, assessment of the proportion between the signal of the non-specific probe and the specific one has been explored in *in vivo* studies using dual probes, where complete wash out of unbound probes is not feasible, and therefore they would contribute to the detected signal [16]. In tissue samples or 3D models of cancer, a simple calibration ratio between the fluorescence recorded from the specific and the negative control probes (similar to our RMA_{FI}-*1* procedure), has been proposed for the removal of fluorescence due to non-specific accumulation of both probes [15]. Nevertheless, those studies have used conventional fluorophores, and their optical properties could be different, particularly their excitation spectra, which requires the use of different sources of excitation light, with different intensities, penetration and scattering patterns. All these could complicate accurate assessment of the ratio between both probes [15,16]. In this study, we assessed *in vitro,* in the confocal stage, the ratio between the FI of both probes based in QD. The multiplexing capacity of QD and confocal microscopy allowed us to acquire their fluorescence simultaneously, in two different channels with similar photomultipliers gain, using the same excitation laser and settings. Nevertheless, a SF needed to be applied to the dimmer QD545 signal in order to normalize its FI to that of the QD605 [17,42], and appropriately perform the RMA_{FI} procedure. RMA_{FI}-*1* yields an estimate of the specific binding of the probe and its spatial distribution in whole BC-MTS optical sections or large ROIs, where the empiric SF, which is an average value from the whole field of view in the microscope, was applied uniformly, yielding accurate estimates. However, when the procedure was applied to single pixels, the intrinsic random variability of the signal (see methods) implies that removal of the non-specific fluorescence might not be 100% accurate for each pixel. Therefore, some pixels which were slightly above 1, upon quantification, could be considered as HER2+ (false positive) and skew the HER2 3D-density, consequently thresholding was required (RMA_{FI}-*1-T*). This allowed us to quantify the pixels presenting the higher contribution of the HER2+ populations, providing an objective HER2 density calculation. By applying RMA_{FI}-*1-T*, pixel-by-pixel, images with minimal non-specific fluorescence, and improved HER2 resolution, were efficiently obtained (Figure 5). Importantly, appropriate removal of non-specific fluorescence with this threshold was supported by the results, since HER2 3D-density in HER2– BC-MTS was ~8–9% in both, the non-permeabilized and the permeabilized groups (Figure 6*A*). The HER2 3D-density in HER2– BC-MTS was attributed to the basal HER2 expression in the MCF-7 cells, which could be resolved due to the high affinity/high quantum yield of the Aff-QD probe, and it is within the range reported by others in these cells. For example, Yezhelyev *et al.* (2007) [17] showed that MCF-7 cells could present up to 24% of HER2 expression, when compared with the HER2+ cell line, BT-474, analyzed by single cell spectroscopy using AB-QD probes. Furthermore, the HER2 3D-density in HER2+ permeabilized BC-MTS was ~48%, which, as expected, was significantly higher than that in the HER2– cells mentioned above. (Figure 6*A*), and which was associated with an IHC score of 3+ (Figure 7*B*), typically observed in this cell line [32].

We showed that two different HER2+ BC-MTS populations, cultured independently, were efficiently discriminated by HER2 3D-density calculation. Nevertheless, a particular problem for HER2

overexpression diagnosis in BC tumors arises from heterogeneity of the protein expression among the cells of the same tissue, which is also a problem for the analysis of other molecular targets in several cancers [14]. Therefore, in order to mimic a heterogeneous HER2 model of BC, a co-culture of HER2– and HER2+ cells was used to yield stable hybrid heterogeneous BC-MTS. 3D co-cultures haven been explored mixing cancer cell lines of specific type and properties, with cell lines of different kind, like macrophages or fibroblast, in order to study tumor migration and proliferation [55,56]. Nevertheless, in this study we contribute with the novelty of co-culture exploration of two cancer cell lines with different molecular targets expression to assess specific HER2 signal quantification in a heterogeneous 3D model of BC. The heterogeneity of the two HER2 populations cells, within the BC-MTS, was confirmed because distinctive cell clusters with non-specific signal, almost completely lacking specific signal (HER2– cells), were present, while other clusters displaying high Affanti-HER2-QD605 signal (HER2+ cells), were observed, within the BC-MTS along all the Z distance recorded (Figure 6*B* and Supplementary Figure 3). This heterogeneous distribution of HER2+ cells within the hybrid BC-MTS was confirmed with conventional IHC analysis performed in parallel experiments (Figure 7*C*). Importantly, after RMA_{FI}-*1-T*, HER2 3D-density in the hybrid BC-MTS yielded an intermediate value between those found in single HER2– and HER2+ populations. Relatively constant values of mean HER2 density were found in every optical section recorded along the Z distance up to 70 μm from the coverslip surface (Figure 6*C*). Although, specific detection of HER2 was achieved in HER2+ Triton-permeabilized BC-MTS up to 100 μm of depth, reduced signal-to-noise ratio beyond 70 μm, due to optical limitation of the confocal microscope [57], could affect the automatized RMA_{FI}-*1-T* analysis performed pixel-by-pixel, obscuring the true fraction of HER2+ pixels. Therefore, an appropriate specific and objective HER2 analysis in BC-MTS, or other thick samples, can only be achieved up to 70 μm of depth. Recently, using secondary detection with AB-fluorophore probes in a protocol which takes ~1.5 days, and exploring the fluorescence using a light sheet-based microscope (which has better penetration than confocal microscopy), specific fluorescence signal up 200 μm within spheroids was described [54]. Since in our study, we were limited by the depth which could be observed by confocal microscopy, using techniques like light sheet-based microscopy or two-photon microscopy, could improve the depth detected for the Aff-QD probes [54,57]. On the other hand, using smaller size QD, could be explored to decrease the size of the resulted Aff-QD probe and assess their penetration within thick samples.

Tumors are complex and heterogeneous 3D structures, where large variability occurs in different locations [14], therefore, accurate assessment of epitopes expression in single optical planes (XY), as well as along the Z distance (to get a 3D distribution), is highly desirable. In this study, the use of BC-MTS allowed us to mimic the complex 3D structure of a human biopsy sample. BC-MTS, are easy to grow and approximate the structure of solid tumors, and provide an opportunity to assess the effect of novel pharmacological tools and epitope detection strategies, and have had solid impact in developing new therapies against cancer [58]. However, less effort has been applied for 3D molecular target screening, where more accessible imaging detection, quantification and automatization in these models remain a challenge [58,59], since visualization of external layers of the 3D model using cytospin procedure [60], or complicate and time-consume histological detection of 2D FFPE sections have been used [61,62], nevertheless, they do not allow a complete 3D reconstruction. Our study was a proof of concept for the automatized detection of HER2+ expression in 3D BC-MTS using multispectral conjugates of Aff and QD to address the subjectivity of HER2+ detection and reduce the processing of the samples. This study demonstrated that HER2 could be efficiently quantified with direct incubation of two Aff-QD probes in minimally processed 3D models of BC, where the typical time-consuming and extensive processing-requiring physical sectioning performed in 2D FFPE sections, was replaced by confocal optical sectioning. With the post-acquisition image processing presented here, objective quantification of HER2 could be achieved in homogenous and heterogeneous BC-MTS, up to ~70 μm of depth. HER2 detection process could be performed within 8 h, from the fixation process of the BC-MTS until the HER2 3D-density calculation by the automatized mathematical process of RMA_{FI}-*1-T*, using the widely available MATLAB software.

Nevertheless, since our study was limited to BC-MTS, to assess the translational capacity of the proposed method, to discriminate HER2 signals in thick samples, these procedures must be assessed in human biopsies, where a more complex environment occurs, and which might determine different accumulation patterns of the Aff-QD probes. Furthermore, typical human biopsies samples are larger (in the XY plane), when compared with BC-MTS, therefore optical magnification of the field used in this study, did not allow to make an extended exploration, affecting the HER2 overexpression detection due to the intrinsically heterogeneity of the sample. Therefore, to avoid missing HER2 expressing areas in large samples, random confocal ROI sampling could be performed, or by sequentially recording multiples ROIs, for post-acquisition reconstruction of the complete XY confocal planes, and this could be performed manually using a grid pattern [63,64] or with an automatized mosaic function [65].

Conclusions

Specific and objective detection of HER2 in a 3D model of a BC sample, with minimal processing, was achieved using novel Aff-QD probes, and mathematical processing by RMA_{FI}-1-T for signal quantification. Conjugation of QD with Aff resulted in nanoscale Aff-QD, highly specific probes that presented excellent penetration properties within BC-MTS. The multiplexing detection of a negative control (Affneg-QD545) and a specific probe for HER2 (Affanti-HER2-QD605), in relatively thick BC-MTS, allowed us to assess the non-specific accumulation of the probes within the sample, which otherwise would lead to false positive signals. RMA_{FI} and thresholding efficiently removed this non-specific signal, allowing specific HER2 detection and objective quantification in homogeneous and heterogeneous BC-MTS. The study proposed here, provided the bases for fast an accurate 3D HER2 detection, with the potential to be applied in research laboratory practice for assessment of drugs effects on HER2 overexpressing cells. More importantly, the method has the potential of clinical translation for detection of HER2 overexpression in thick BC tissue samples or even *in vivo*, where, washing off the probes could be complicate.

Conflict of Interests

The authors declare that they do not have any conflict of interest.

Acknowledgements

J. Altamirano and N. García are professors ascribed to the Strategic Focus Group in Cardiovascular Medicine and Metabolomics, School

of Medicine, Tecnologico de Monterrey. Their research was performed at the research facilities of the School of Medicine, Hospital Zambrano Hellion, and CITES (Center for Innovation and Transference in Health), Tecnologico de Monterrey.

This work was supported by grants from SEP-CONACYT: Projects 156717 (J. Altamirano) and 181460 (N. García), and a scholarship from CONACyT and the Tecnologico de Monterrey to P. Pérez-Treviño. We thank Dr. Sean Scott for allowing us to use his cell culture facilities and for helpful discussions.

Appendix A. Supplementary Data

Supplementary data to this article can be found online at https://doi.org/10.1016/j.tranon.2018.03.004.

References

[1] Ross JS, Slodkowska EA, Symmans WF, Pusztai L, Ravdin PM, and Hortobagyi GN (2009). The HER-2 receptor and breast cancer: ten years of targeted anti-HER-2 therapy and personalized medicine. *Oncologist* **14**(4), 320–368.

[2] Tai W, Mahato R, and Cheng K (2010). The role of HER2 in cancer therapy and targeted drug delivery. *J Control Release* **146**(3), 264–275.

[3] Cancer Genome Atlas Network (2012). Comprehensive molecular portraits of human breast tumours. *Nature* **490**(7418), 61–70.

[4] Kohler BA, Sherman RL, Howlader N, Jemal A, Ryerson AB, Henry KA, Boscoe FP, Cronin KA, Lake A, and Noone AM, et al (2015). Annual report to the nation on the status of cancer, 1975-2011, featuring incidence of breast cancer subtypes by race/ethnicity, poverty, and state. *J Natl Cancer Inst* **107**(6), 1–25.

[5] Joensuu H (2017). Escalating and de-escalating treatment in HER2-positive early breast cancer. *Cancer Treat Rev* **52**, 1–11.

[6] Cardinale D, Colombo A, Torrisi R, Sandri MT, Civelli M, Salvatici M, Lamantia G, Colombo N, Cortinovis S, and Dessanai MA, et al (2010). Trastuzumab-induced cardiotoxicity: clinical and prognostic implications of troponin I evaluation. *J Clin Oncol* **28**(25), 3910–3916.

[7] Bonifazi M, Franchi M, Rossi M, Moja L, Zambelli A, Zambon A, Corrao G, La Vecchia C, Zocchetti C, and Negri E (2013). Trastuzumab-related cardiotoxicity in early breast cancer: a cohort study. *Oncologist* **18**(7), 795–801.

[8] Perez EA, Suman VJ, Davidson NE, Martino S, Kaufman PA, Lingle WL, Flynn PJ, Ingle JN, Visscher D, and Jenkins RB (2006). HER2 testing by local, central, and reference laboratories in specimens from the north central cancer treatment group N9831 intergroup adjuvant trial. *J Clin Oncol* **24**(19), 3032–3038.

[9] Wolff AC, Hammond ME, Hicks DG, Dowsett M, McShane LM, Allison KH, Allred DC, Bartlett JM, Bilous M, and Fitzgibbons P, et al (2013). Recommendations for human epidermal growth factor receptor 2 testing in breast cancer: American Society of Clinical Oncology/College of American Pathologists clinical practice guideline update. *J Clin Oncol* **31**(31), 3997–4013.

[10] Jacobs TW, Gown AM, Yaziji H, Barnes MJ, and Schnitt SJ (1999). Specificity of HercepTest in determining HER-2/neu status of breast cancers using the United States Food and Drug Administration–approved scoring system. *J Clin Oncol* **17**(7), 1983–1987.

[11] Paik S, Bryant J, Tan-Chiu E, Romond E, Hiller W, Park K, Brown A, Yothers G, Anderson S, and Smith R, et al (2002). Real-world performance of HER2 testing—national surgical adjuvant breast and bowel project experience. *J Natl Cancer Inst* **94**(11), 852–854.

[12] Bahreini F, Soltanian AR, and Mehdipour P (2015). A meta-analysis on concordance between immunohistochemistry (IHC) and fluorescence in situ hybridization (FISH) to detect HER2 gene overexpression in breast cancer. *Breast Cancer* **22**(6), 615–625.

[13] Perez EA, Cortés J, Gonzalez-Angulo AM, and Bartlett JMS (2014). HER2 testing: current status and future directions. *Cancer Treat Rev* **40**(2), 276–284.

[14] Potts SJ, Young GD, and Voelker FA (2010). The role and impact of quantitative discovery pathology. *Drug Discov Today* **15**(21/22), 943–950.

[15] Liu JTC, Helms MW, Mandella MJ, Crawford JM, Kino GS, and Contag CH (2009). Quantifying cell-surface biomarker expression in thick tissues with ratiometric three-dimensional microscopy. *Biophys J* **96**(6), 2405–2414.

[16] Tichauer KM, Samkoe KS, Sexton KJ, Hextrum SK, Yang HH, Klubben WS, Gunn JR, Hasan T, and Pogue PW (2012). In vivo quantification of tumor receptor binding potential with dual-reporter molecular imaging. *Mol Imaging Biol* **14**(5), 584–592.

[17] Yezhelyev MV, Al-Hajj A, Morris C, Marcus AI, Liu T, Lewis M, Cohen C, Zrazhevskiy P, Simons JW, and Rogatko A, et al (2007). In situ molecular profiling of breast cancer biomarkers with multicolor quantum dots. *Adv Mater* **19**(20), 3146–3151.

[18] Tiwari DK, Tanaka S-I, Inouye Y, Yoshizawa K, Watanabe TM, and Jin T (2009). Synthesis and characterization of anti-HER2 antibody conjugated CdSe/CdZnS quantum dots for fluorescence imaging of breast cancer cells. *Sensors (Basel)* **9**(11), 9332–9364.

[19] Chen C, Peng J, Xia H, Wu Q, Zeng L, Xu H, Tang H, Zhang Z, Zhu X, and Pang D, et al (2010). Quantum-dot-based immunofluorescent imaging of HER2 and ER provides new insights into breast cancer heterogeneity. *Nanotechnology* **21**(9), 1–6.

[20] Liu XL, Peng CW, Chen C, Yang XQ, Hu MB, Xia HS, Liu SP, Pang DW, and Li Y (2011). Quantum dots-based double-color imaging of HER2 positive breast cancer invasion. *Biochem Biophys Res Commun* **409**(3), 577–582.

[21] Zrazhevskiy P, Sena M, and Gao X (2010). Designing multifunctional quantum dots for bioimaging, detection, and drug delivery. *Chem Soc Rev* **39**(11), 4326–4354.

[22] Liu J, Lau SK, Varma VA, Moffitt RA, Caldwell M, Liu T, Young AN, Petros JA, Osunkoya AO, and Krogstad T, et al (2010). Molecular mapping of tumor heterogeneity on clinical tissue specimens with multiplexed quantum dots. *ASC Nano* **4**(5), 2755–2765.

[23] Gao J, Chen K, Miao Z, Ren G, Chen X, Gambhir SS, and Cheng Z (2011). Affibody-based nanoprobes for HER2-expressing cell and tumor imaging. *Biomaterials* **32**(8), 2141–2148.

[24] Zhao N, Liu S, Jiang Q, Lan T, Cheng Z, and Liu H (2016). Small-protein-stabilized semiconductor nanoprobe for targeted imaging of cancer cells. *Chembiochem* **17**(3), 1202–1206.

[25] Ståhl S, Gräslund T, Eriksson KA, Frejd FY, Nygren PA, and Löfblom J (2017). Affibody molecules in biotechnological and medical applications. *Trends Biotechnol* **35**(8), 691–712.

[26] Löfblom J, Feldwisch J, Tolmachev V, Carlsson J, Ståhl S, and Frejd FY (2010). Affibody molecules: Engineered proteins for therapeutic, diagnostic and biotechnological applications. *FEBS Lett* **584**(12), 2670–2680.

[27] Zielinski R, Hassan M, Lyakhov I, Needle D, Chernomordik V, Garcia-Glaessner A, Ardeshirpour Y, Capala J, and Gandjbakhche A (2012). Affibody-DyLight conjugates for in vivo assessment of HER2 expression by near-infrared optical imaging. *PLoS One* **7**(7), 1–10.

[28] Sandstrom M, Lindskog K, Velikyan I, Wennborg A, Feldwisch J, Sandberg D, Tolmachev V, Orlova A, Jens S, and Carlsson J, et al (2016). Biodistribution and radiation dosimetry of the anti-HER2 affibody molecule 68Ga-ABY-025 in breast cancer patients. *J Nucl Med* **57**(6), 867–871.

[29] Sorensen J, Sandberg D, Sandstrom M, Wennborg A, Feldwisch J, Tolmachev V, Astrom G, Lubberink M, Garske-Roman U, and Carlsson J, et al (2014). First-in-Human molecular imaging of HER2 expression in breast cancer metastases using the 111In-ABY-025 affibody molecule. *J Nucl Med* **55**(5), 730–735.

[30] Edmondson R, Broglie JJ, Adcock AF, and Yang L (2014). Three-dimensional cell culture systems and their applications in drug discovery and cell-based biosensors. *Assay Drug Dev Technol* **12**(4), 207–218.

[31] Gazdar AF, Kurvari V, Virmani A, Gollahon L, Sakaguchi M, Westerfield M, Kodagoda D, Stasny V, Cunningham HT, and Wistuba II, et al (1998). Characterization of paired tumor and non-tumor cell lines established from patients with breast cancer. *Int J Cancer* **78**(6), 766–774.

[32] Clinchy B, Gazdar A, Rabinovsky R, Yefenof E, Gordon B, and Vitetta ES (2000). The growth and metastasis of human, HER-2 / neu-overexpressing tumor cell lines in male SCID mice. *Breast Cancer Res Treat* **61**(3), 217–228.

[33] Subik K, Lee JF, Baxter L, Strzepek T, Costello D, Crowley P, Xing L, Hung MC, Bonfiglio T, and Hicks DG, et al (2010). The expression patterns of ER, PR, HER2, CK5/6, EGFR, KI-67 and AR by immunohistochemical analysis in breast cancer cell lines. *Breast Cancer (Auckl)* **4**(1), 35–41.

[34] Xiao Y, Gao X, Maragh S, Telford WG, and Tona A (2009). Cell lines as candidate reference materials for quality control of ERBB2 amplification and expression assays in breast cancer. *Clin Chem* **55**(7), 1307–1315.

[35] Imamura Y, Mukohara T, Shimono Y, Funakoshi Y, Chayahara N, Toyoda M, Kiyota N, Takao S, Kono S, and Nakatsura T, et al (2015). Comparison of 2D- and 3D-culture models as drug-testing platforms in breast cancer. *Oncol Rep* **33**(4), 1837–1843.

[36] Pervin S, Hewison M, Braga M, Tran L, Chun R, Karam A, Chaudhuri G, Norris K, and Singh R (2013). Down-regulation of vitamin D receptor in mammospheres: implications for vitamin D resistance in breast cancer and potential for combination therapy. *PLoS One* **8**(1), 1–15.

[37] Weiswald L, Bellet D, and Dangles-Marie V (2015). Spherical cancer models in tumor biology. *Neoplasia* **17**(1), 1–15.

[38] Park Y, Ryu YM, Jung Y, Wang T, Baek Y, Yoon Y, Bae SM, Park J, Hwang S, and Kim J, et al (2014). Spraying quantum dot conjugates in the colon of live animals enabled rapid and multiplex cancer diagnosis using endoscopy. *ACS Nano* **8**(9), 8896–8910.

[39] Rizvi SB, Rouhi S, Taniguchi S, Yang SY, Green M, Keshtgar M, and Seifalian AM (2014). Near-infrared quantum dots for HER2 localization and imaging of cancer cells. *Int J Nanomedicine* **9**(1), 1323–1337.

[40] Gostring L, Malm M, Höidén-Guthenberg I, Frejd FY, Ståhl S, Löfblom J, and Gedda L (2012). Cellular effects of HER3-specific affibody molecules. *PLoS One* **7**(6), 1–9.

[41] Schindelin J, Arganda-Carreras I, Frise E, Kaynig V, Longair M, Pietzsch T, Preibisch S, Rueden C, Saalfeld S, and Schmid B, et al (2012). Fiji: an open-source platform for biological-image analysis. *Nat Methods* **9**(7), 676–682.

[42] Huang D, Peng X, Su L, Wang D, Khuri FR, Shin DM, and Chen Z (2010). Comparison and optimization of multiplexed quantum dot-based immunohisto-fluorescence. *Nano Res* **3**(1), 61–68.

[43] Orlova A, Magnusson M, Eriksson TLJ, Nilsson M, Larsson B, Hoiden-Guthenberg I, Widstrom C, Carlsson J, Tolmachev V, and Stahl S, et al (2006). Tumor imaging using a picomolar affinity HER2 binding affibody molecule. *Cancer Res* **66**(8), 4339–4348.

[44] Lundberg E, Höidén-Guthenberg I, Larsson B, Uhlen M, and Graslund T (2007). Site-specifically conjugated anti-HER2 Affibody® molecules as one-step reagents for target expression analyses on cells and xenograft samples. *J Immunol Methods* **319**(1–2), 53–63.

[45] Tada H, Higuchi H, Wanatabe TM, and Ohuchi N (2007). In vivo real-time tracking of single quantum dots conjugated with monoclonal anti-HER2 antibody in tumors of mice. *Cancer Res* **67**(3), 1138–1144.

[46] Takeda M, Tada H, Higuchi H, Kobayashi Y, Kobayashi M, Sakurai Y, Ishida T, and Ohuchi N (2008). In vivo single molecular imaging and sentinel node navigation by nanotechnology for molecular targeting drug-delivery systems and tailor-made medicine. *Breast Cancer* **15**(2), 145–152.

[47] Rudnick SI, Lou J, Shaller CC, Tang Y, Klein-Szanto AJP, Weiner LM, Marks JD, and Adams GP (2011). Influence of affinity and antigen internalization on the uptake and penetration of anti-HER2 antibodies in solid tumors. *Cancer Res* **71**(6), 2250–2259.

[48] Vaneycken I, Devoogdt N, Gassen NV, Vincke C, Xavier C, Wernery U, Muyldermans S, Lahoutte T, and Caveliers V (2011). Preclinical screening of anti-HER2 nanobodies for molecular imaging of breast cancer. *FASEB J* **25**(7), 2433–2446.

[49] Rudnick SI and Adams GP (2009). Affinity and Avidity in Antibody-Based Tumor Targeting. *Cancer Biother Radiopharm* **24**(2), 155–161.

[50] Tichauer KM, Diop M, Elliott JT, Samkoe KS, Hasan T, St. Lawrence K, and Pogue BW (2014). Accounting for pharmacokinetic differences in dual-tracer receptor density imaging. *Phys Med Biol* **59**(10), 2341–2351.

[51] Li Y, Zhang R, Han Y, Lu T, Ding J, Zhang K, Lin G, Xie J, and Li J (2016). Comparison of the types of candidate reference samples for quality control of human epidermal growth factor receptor 2 status detection. *Diagn Pathol* **11**(85), 1–9.

[52] Amidzadeh Z, Behbahani AB, Erfani N, Sharifzadeh S, Ranjbaran R, Moezi L, Aboualizadeh F, Okhovat MA, Alavi P, and Azarpira N (2014). Assessment of different permeabilization methods of minimizing damage to the adherent cells for detection of intracellular RNA by flow cytometry. *Avicenna J Med Biotechnol* **6**(1), 38–46.

[53] Weiswald LB, Guinebretière JM, Richon S, Bellet D, Saubaméa B, and Dangles-Marie V (2010). In situ protein expression in tumour spheres: development of an immunostaining protocol for confocal microscopy. *BMC Cancer* **10**(1), 1–11.

[54] Smyrek I and Stelzer EHK (2017). Quantitative three-dimensional evaluation of immunofluorescence staining for large whole mount spheroids with light sheet microscopy. *Biomed Opt Expr* **8**(2), 484–499.

[55] Linde N, Gutschalk CM, Hoffmann C, Yilmaz D, and Mueller MM (2012). Integrating macrophages into organotypic co-cultures: a 3D in vitro model to study tumor-associated macrophages. *PLoS One* **7**(7), 1–13.

[56] Kim SA, Lee EK, and Kuh HJ (2015). Co-culture of 3D tumor spheroids with fibroblasts as a model for epithelial – mesenchymal transition in vitro. *Exp Cell Res* **335**(2), 187–196.

[57] Combs CA (2010). Fluorescence microscopy: A concise guide to current imaging methods. *Curr Protoc Neurosci* , 1–19.

[58] Fang Y and Eglen RM (2017). Three-dimensional cell cultures in drug discovery and development. *SLAS Discov* **22**(5), 456–472.

[59] Li L, Zhou Q, Voss TC, Quick KL, and LaBarbera DV (2016). High-throughput imaging: focusing in on drug discovery in 3D. *Methods* **96**(1), 97–102.

[60] Toma JG, McKenzie IA, Bagli D, and Miller FD (2005). Isolation and characterization of multipotent skin-derived precursors from human skin. *Stem Cells* **23**(6), 727–737.

[61] Cheng V, Esteves F, Chakrabarty A, Cockle J, and Short S (2015). High-content analysis of tumour cell invasion in three-dimensional spheroid assays. *Oncoscience* **2**(6), 596–606.

[62] Nagelkerke A, Bussink J, Sweep FCGJ, and Span PN (2013). Generation of multicellular tumor spheroids of breast cancer cells: how to go three-dimensional. *Anal Biochem* **437**(1), 17–19.

[63] Dobbs JL, Ding H, Benveniste AP, Kuerer HM, Krishnamurthy S, Yang W, and Richards-Kortum R (2013). Feasibility of confocal fluorescence microscopy for real-time evaluation of neoplasia in fresh human breast tissue. *J Biomed Opt* **18**(10), 1–10.

[64] Dobbs J, Krishnamurthy S, Kyrish M, Benveniste AP, Yang W, and Richards-Kortum R (2015). Confocal fluorescence microscopy for rapid evaluation of invasive tumor cellularity of inflammatory breast carcinoma core needle biopsies. *Breast Cancer Res Treat* **149**, 303–310.

[65] Bini J, Spain J, Nehal K, Hazelwood V, DiMarzio C, and Rajadhyaksha M (2011). Confocal mosaicing microscopy of human skin ex vivo: spectral analysis for digital staining to simulate histology-like appearance. *J Biomed Opt* **16**(7), 1–8.